# **Experimental characterisation of lateral thrust jets** for subsonic missile configurations

T. Gawehn, P. Gruhn, A. Gülhan 1

#### **Abstract**

The LK6E2 is designed by DLR as a missile against ground or low flying targets. It operates at low altitude and high subsonic velocities. The missile is boosted by four lateral thrust nozzles at its tail while aerodynamic forces and moments are generated via four main and four rear wings (fins). The aim of the current study is to assess experimentally a potential interaction of the thrust jets on the control surfaces. As this problem cannot be directly assessed, a stepwise approach is used: Based on similarity rules, a cold gas model is designed and investigated with Pressure Sensitive Paint (PSP) and Particle Image velocimetry (PIV) first. Then, same rules are applied to design a hot gas model to be used with a solid propellant suitable for wind tunnel experiments. Hot gas PIV is applied and results are compared with the cold gas case. Additionally, flow visualisation is performed by means of Schlieren imaging. Finally, a combined analysis of all experimental results should allow for a transfer of the findings to the real configuration, but this is a future step and not yet addressed herein.

**Keywords:** Lateral thrust jets, Wind tunnel testing, Pressure Sensitive Paint (PSP), Particle Image Velocimetry (PIV), Supersonic jet in cross-flow

# **Nomenclature**

Latin		$\kappa$	Ratio of specific heats
Α	Area	ρ	Density
С	Coefficient	Φ	Roll angle
D	Diameter		-
F	Thrust	Subscr	ipts
Н	Altitude	С	Combustion
L	Length	CC	Combustion chamber
Ma	Mach number	in	inner
R	Gas constant	j	Jet
m	Mass	ne	Nozzle exit
р	Pressure	nt	Nozzle throat
q	Dynamic pressure	out	outer
Τ	Temperature	р	Pressure
u,V	Velocity	t	Total condition
		th.	theoretical
Greek		Wt	Wind tunnel
δ	Inclination angle of thrust nozzle	0	Stagnation condition
$\varepsilon$	Area/expansion ratio	∞	Freestream condition
η	Efficiency		

<sup>&</sup>lt;sup>1</sup> German Aerospace Center (DLR), Institute of Aerodynamics and Flow Technology, Supersonic and Hypersonic Technologies Department, Linder Höhe, 51147 Köln, Germany, Thomas.gawehn@dlr.de

HiSST-2025-0084 Page 1 | 16 Experimental characterisation of lateral thrust jets for subsonic missile configurations Copyright © 2025 by author(s)

#### 1. Introduction

Research conducted at DLR focuses on missile technology, utilizing generic reference missile configurations that are tailored to specific research topics and representative of various missile classes. This study employs both numerical and experimental analysis to investigate the aerodynamic performance of these missile configurations. One such configuration is Reference Configuration 6 (LK6), which is designed as a highly agile missile capable of operating at high subsonic velocities. The LK6 is propelled by a rocket motor that utilizes lateral thrust nozzles, while aerodynamic forces and moments are generated by a combination of wings and fins. One aspect to be investigated is a potential interaction between the thrust jets and the downstream fins. This might influence fin efficiency and, consequently, the overall aerodynamic properties of the missile.

#### 1.1. HIGHLY AGILE SUBSONIC MISSILE - REFERENCE CONFIGURATION LK6

The LK6 is a reference configuration designed by DLR for a highly agile, high subsonic missile suitable for defence against ground and air targets operating at moderate speeds at low altitudes. It is powered by a rocket motor and achieves a maximum range of around  $8\,km$  via four laterally arranged thrust nozzles. It is guided into the target optically, via IR or via radar. A connection via fibre optics in the rear provides control throughout the complete mission.

The missile has an overall length of  $L=1.5\,m$  and a diameter of  $D=0.15\,m$ , with a blunt tangent nose. The aerodynamic forces and moments are generated by four main wings and four rear wings (fins). The wings are not arranged equidistantly in the circumferential direction, which gives the missile an aerodynamically favourable plane. The leading and trailing edges of the wings and fins are designed as semicircles. Due to the arrangement, an interaction between the lateral thrust jets and the downstream fins may occur, influence fin efficiency and, consequently, the overall aerodynamic properties of the missile.

Within this study, the version E2 of the reference configuration shown in Fig. 1 is investigated.

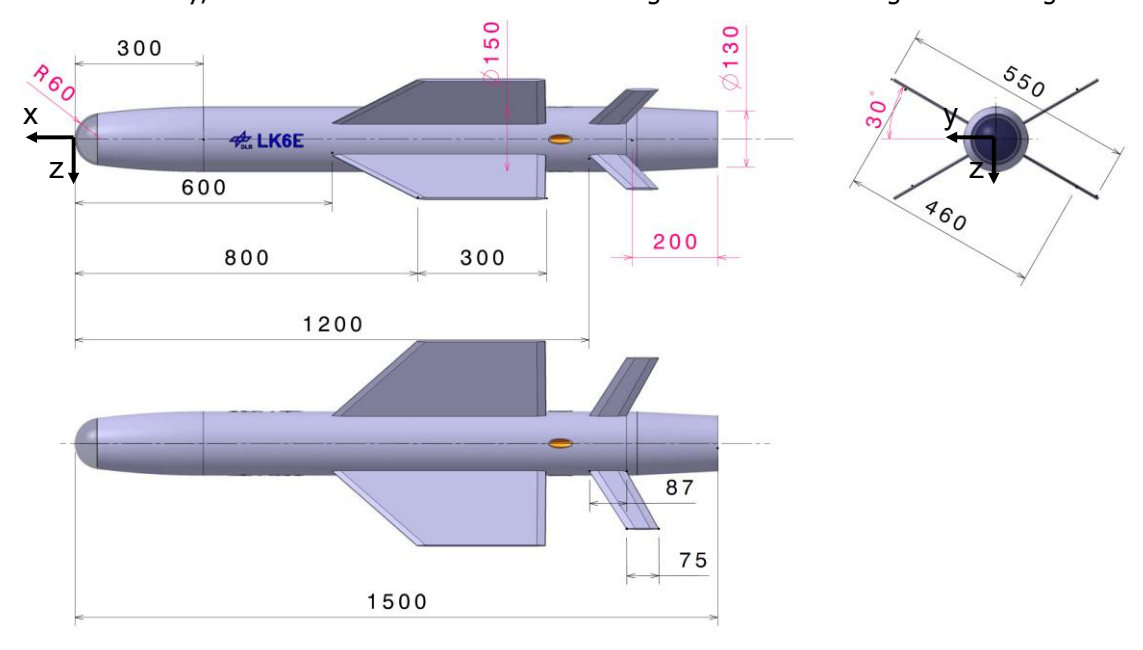


Fig. 1. Reference configuration LK6 in version E2 [1]

#### 1.2. REFERENCE MISSION

The mission against a ground object shown in Fig. 2 is assumed to be the reference mission for the design of the thrusters of the LK6E2. The start mass of the missile is about m=50~kg. The flight duration is approx. 40 seconds and the missile reaches a maximum flight speed of  $Ma\approx0.85$ . During the launch phase, a strong acceleration is achieved with a total thrust of  $F\approx2400~N$ . After about 5 seconds at a velocity of Ma>0.6, the thrust is reduced to  $F\approx400~N$  for the remainder of the mission, further accelerating the missile. The maximum altitude achieved is  $H\approx0.3~km$ .

Fig. 2. Reference mission of LK6E2 against ground target

#### 1.3. THRUST NOZZLE DESIGN

For a simplified thrust nozzle design for LK6E2, a propellant consisting of 69% Ammoniumperchlorat, 19% Aluminium and 12% Hydroxyl-terminated Polybutadien is assumed. The software tool Rocket Propulsion Analysis (RPA) in Version 1.2.9 Lite Edition (win32-version) is applied for first estimations. Then, a one-dimensional gas dynamic analysis is performed considering a gas constant of R =269 J/kgK and a ratio of specific heats of  $\kappa = 1.156$ . For the start phase, stagnation conditions of the gas of  $p_{0,CC}=11.8\,MPa$ ,  $T_{0,CC}=3605\,K$  are assumed. By specifying an area ratio (here:  $\varepsilon_{Target}\approx5$ ), the Mach number at the exit of the nozzle, which is assumed to be conical ( $Ma_i = 2.71$ ), is determined. A combustion efficiency of  $\eta_C = 0.92$  is assumed. The inclination angle of the nozzle relative to the longitudinal axis (here:  $\delta = 22.5^{\circ}$ ) finally gives the axial thrust. The diameter at the exit is adjusted so that the desired axial thrust for the start phase (here:  $F_{Target} = 2400 N$ , see reference mission in Fig. 2) is achieved. It is  $D = 0.0309 \, m$ . The thrust, i.e. the required area, is then equally distributed over the four nozzles. As a result, each nozzle has a cross-section at the exit of  $D_{\rm ne}=15.43~mm$  and in the nozzle throat of  $D_{\rm nt} = 6.88 \ mm$ . The reduced thrust for the cruise phase (here:  $F_{\rm Target} = 400 \ N$ ) requires a combustion chamber pressure of  $p_{0,CC} = 2.24 \, MPa$ . In addition, an intermediate Phase is defined with a thrust of  $F_{\rm Target} = 1400 \, N$  and the corresponding combustion chamber pressure of  $p_{0.CC} = 7.10 MPa$ .

#### 1.4. APPROACH

The current experimental study focuses on the investigation of the thrust jets and a potential interference with control surfaces. In a first step, the hot gas is simulated with cold gas to allow for the application of certain investigation techniques. For that purpose, the thrust nozzles of the wind tunnel model are designed applying similarity rules. A cold gas wind tunnel model is built and researched. Then, investigations are performed in the wind tunnel using real propellants, but with a different composition than the original one. Design of the nozzles for this model also required the application of similarity rules. Finally, a combination of the results aims to predict the conditions for the original configuration.

# 1.5. CONTENT OF THIS PAPER

The investigation of the LK6E2 is ongoing. This publication presents an extract of the experimental results available from different experimental test campaigns. In the frame of this publication, only an extract of the results can be presented.

# 2. EXPERIMENTAL SETUP

# 2.1. VERTICAL TEST SECTION COLOGNE (VMK)

The vertical test section Cologne (VMK) is shown schematically in Fig. 3, left. Compressed, dried air from a reservoir is fed to the nozzle via settling chamber and several rectifier screens. Depending on the requirements, supersonic or subsonic nozzles are used, that exit to a vertical free jet test section. The achievable Mach numbers are in the range of  $0.5 \le Ma \le 3.2$ . The stagnation pressure of the flow can be adjusted up to a pressure of  $p_0=3.5\,\mathrm{MPa}$ . The flow can also be heated to stagnation temperatures of up to  $T_0 = 750 \, K$  within the storage heater. This allows aerothermodynamic loads up

to Ma = 2.8 to be exactly duplicated under near-ground conditions in order to aerothermally characterise missiles and spacecraft and to qualify individual components for flight.

Three different axis-symmetric nozzles with an exit diameter of  $184\,mm$ ,  $270\,mm$  and  $340\,mm$  are available for subsonic tests. In the supersonic range, VMK facilitates tests with 14 axis-symmetric nozzles exhibiting an exit diameter of  $150\,mm$ ,  $230\,mm$  and  $310\,mm$ . A subsonic nozzle with an exit diameter of  $340\,mm$  is used for the current investigations. An axially symmetrical model holder with the option of supplying a blow-out medium and/or measuring lines, e.g. for pressure or temperature measurements in the model, is located in the centre of the nozzle.

In the subsonic range, a Prandtl probe is usually positioned in the area of the nozzle exit in order to calculate the Mach number from the ratio of dynamic pressure  $q_{\infty}$  and static pressure  $p_{\infty}$ . The stagnation pressure  $p_0$  of the wind tunnel is then adjusted to set the Mach number as desired. When performing tests without probe, the total pressure loss  $q_{\infty}/p_0$  from the location where the stagnation pressure is measured to the location of the probe must be determined – it depends on the rectifier screens and the installed model – and considered when controlling the wind tunnel flow only via the stagnation pressure.

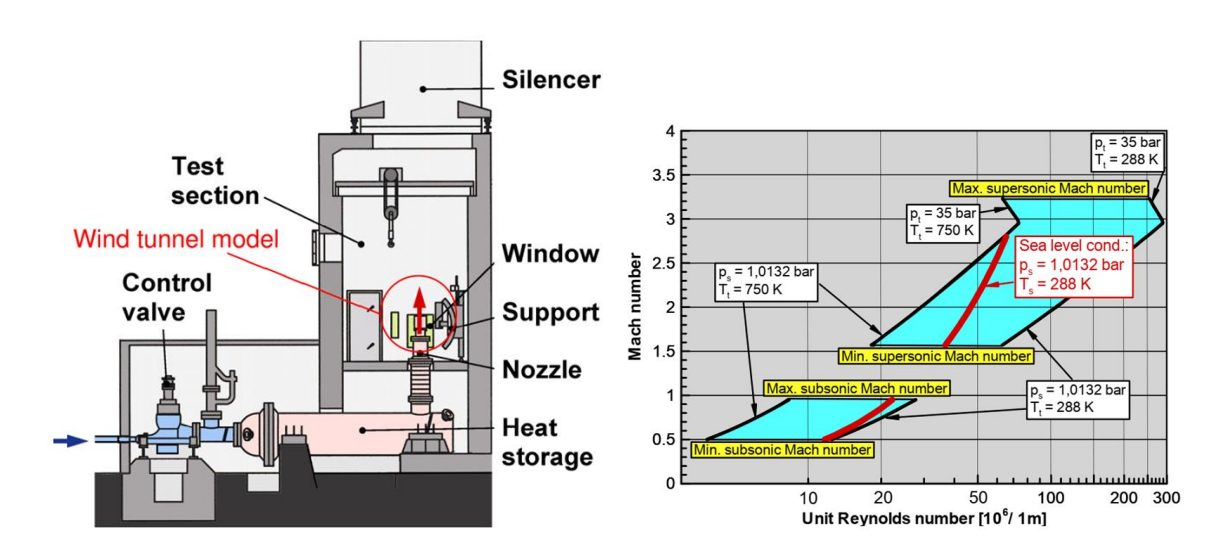


Fig. 3. Schematic (left) and performance map (right) of wind tunnel VMK [2]

## 2.2. WIND TUNNEL MODELS

The scaling factor of LK6E2 for investigations in the VMK is  $1:2.174~(\cong 0.46)$  as the models are to be placed on an existing central model mount in the nozzle. Thereby, general model dimensions are set and the length of the cylindrical part is adjusted to bring the thrust nozzle region above the wind tunnel nozzle's exit.

# Thrust nozzle design

Design of the thrust nozzles is based on similarity parameters published by Pindzola [3]. It is not possible to reproduce all similarity parameters simultaneously in the experiment. Pindzola recommends duplicating the jet *turning angle similarity* in addition to the jet *pressure ratio*, especially for investigations that are limited to the area of the jet exit. On the other hand, for investigations involving the effect on model surfaces in the vicinity of the jet, the *pressure ratio* and the *momentum ratio* of the jet stream are the most important parameters as the momentum remains constant over the course of the jet, while other flow parameters such as velocity, temperature or mass flow rate change.

Applied to the planned flow visualisation using Particle Image Velocimetry (PIV), a reproduction of the jet *pressure ratio* and jet *turning angle* seems advisable. With regard to the surface pressure visualisation on control surfaces by means of Pressure Sensitive Paint (PSP), a reproduction of jet *pressure ratio* and *momentum ratio* should be aimed for. Additionally, flow parameters of the free stream should be reproduced.

A comprehensive study covered all similarity rules proposed by Pindzola [3]. A similarity with regard to *kinetic energy, internal energy* and *enthalpy* cannot be achieved because of the highly different temperatures of hot gas and cold air that are directly incorporated into the similarity parameters and cannot be compensated for by other parameters. The *mass flow similarity* leads to a very small nozzle diameter and the *thrust similarity* parameter, if fitted to the start phase, is no longer fulfilled when the combustion chamber pressure is lowered to simulate the cruise phase.

Finally, the following similarity rules are applied for designing the thrust nozzle geometry:

Turning angle similarity 
$$\left( \frac{p_{j} \cdot \kappa_{j} \cdot M a_{j}^{2}}{p_{\infty} \cdot \kappa_{\infty} \cdot M a_{\infty}^{2}} \frac{\sqrt{M a_{\infty}^{2} - 1}}{\sqrt{M a_{j}^{2} - 1}} \right)_{Wt} = \left( \frac{p_{j} \cdot \kappa_{j} \cdot M a_{j}^{2}}{p_{\infty} \cdot \kappa_{\infty} \cdot M a_{\infty}^{2}} \frac{\sqrt{M a_{\infty}^{2} - 1}}{\sqrt{M a_{j}^{2} - 1}} \right)_{Flight}$$
 (1)

Momentum similarity 
$$\left( \frac{(\rho \cdot u^2 \cdot A)_j}{(\rho \cdot u^2 \cdot A)_\infty} \right)_{Wt} = \left( \frac{(\rho \cdot u^2 \cdot A)_j}{(\rho \cdot u^2 \cdot A)_\infty} \right)_{Flight}$$
 (2)

Pressure ratio similarity 
$$\left(\frac{p_j}{p_\infty}\right)_{Wt} = \left(\frac{p_j}{p_\infty}\right)_{Flight}$$
 (3)

The Mach number  $Ma_j$  at the thrust nozzle's exit, i.e. the expansion ratio  $\varepsilon$ , the diameter at the nozzle exit  $D_{\rm ne}$  and the pressure in the combustion chamber  $p_{0,CC}$  are design parameters.

# Cold gas model

The combustion efficiency for cold gas experiments with the medium dried air is set to  $\eta_c=1.0$ . Reproduction of the jet pressure ratio gives a pressure in the combustion chamber of  $p_{0,CC}=3.988~MPa$  (start phase) resp.  $p_{0,CC}=0.757~MPa$  (cruise phase). The Mach number is determined to  $Ma_j=2.14$  so that the *turning angle similarity* is optimally fulfilled with a deviation of  $\pm 0.45~\%$  for both, start and cruise phase. Then, the *momentum similarity* defines the nozzle geometry with the reference surface  $A_{\infty}$  for the external flow assumed as a quarter of a ring segment, which is limited inwards by the missile  $(D_{in}=0.15~m)$  and outwards by  $D_{out}=0.25~m$ , for the flight case. For the wind tunnel case, these values are scaled. The diameter at the nozzle throat is determined to  $D_{nt}=5.93~mm$  and at the nozzle exit to  $D_{ne}=8.18~mm$ .

### Hot gas model

The aim of hot gas tests is to visualise the interaction of the hot jet with the flow around the model and interactions with control surfaces (fins) using PIV. In order to optimally simulate the thrust jet, it should have a similar gas composition to the exhaust jet of LK6E2 in real flight, i.e. solid propellants are used in the experiment. However, in order to allow for PIV measurements, a significantly reduced aluminium content is required compared to the design propellant.

Two different propellants are available: One consists of 82% Ammoniumperchlorat and 2% Aluminium and the other of 80% Ammoniumperchlorat and 4% Aluminium. Both include 16% Hydroxyl-terminated Polybutadien. Other ingredients are neglected within this simplified analysis. The chemical reaction in the combustion chamber and the flow conditions in the nozzle are estimated using the tool RPA v.1.2.9 Lite Edition. The parameters used for the one-dimensional gas dynamic analysis are a gas constant of  $R_{2\%}=335.7~\frac{J}{kgK}~/~R_{4\%}=331.4~\frac{J}{kgK}$ , a ratio of specific heats of  $\kappa_{2\%}=1.237~/~\kappa_{4\%}=1.233$  and a stagnation temperature of  $T_{0,CC,2\%}=2804~K~/~T_{0,CC,4\%}=2875~K$ .

When using solid propellants, the combustion chamber pressure  $p_{0,CC}$  is not a design parameter any more. It is a function of the minimal cross-section of the outflow (if sonic conditions are reached). An empirical relation based on experiments with a model combustion chamber and exhaust nozzle with defined throat cross-section  $A_{nt}$  is developed. The propellant grains used have the approx. dimensions  $\emptyset$   $46 \ mm \ x \ L \ 84 \ mm$ . Nozzles with different diameter are installed and either one or two grains (if marked accordingly) ignited. The measured data ("Exp.") are shown in Fig. 4 together with relations derived from an exponential curve fit and calculated data beyond the test range ("Calc."). Thereby, an average pressure of the tests and not the maximum pressure is referenced.

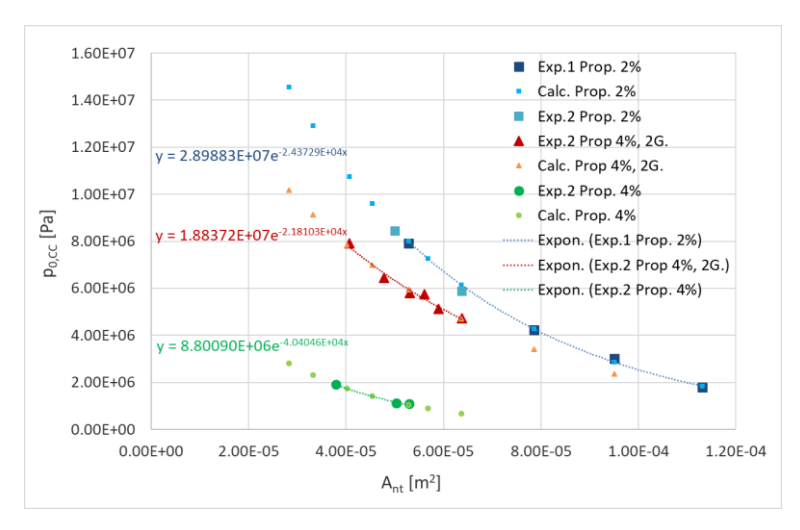


Fig. 4. Combustion chamber pressure po,cc in dependency of nozzle throat area Ant

Within the design of the hot gas model, the inverse functions are used to determine the nozzle throat cross-section  $A_{nt}$  that corresponds to the desired combustion chamber pressure  $p_{0,cc}$ . The determined area is then distributed on the number of nozzles. The same similarity parameters than above, are applied to design the nozzles. Since the combustion chamber pressure is no longer an independent design parameter, the *start* and *cruise phase* cannot be realised with identical nozzle geometries.

Application of *momentum*, *thrust* and *mass flow similarity* on the thrust nozzle geometry gives a pressure in the combustion chamber for the start phase of  $p_{0,CC} \ge 17~MPa$  which is regarded as too high to perform experiments safely. The *turning angle similarity* instead, results in an acceptable combustion chamber pressure of  $p_{0,CC} = 7.381~MPa$ , a Mach number of  $Ma_j = 2.50$  and a nozzle throat diameter of  $D_{nt} = 4.23~mm$  for four identical nozzles.

To overcome the issue of a necessary change in nozzle geometry to simulate the *cruise phase*, two approaches are tried: First, 3 nozzles are designed identical and the 4<sup>th</sup> auxiliary nozzle is adapted. Second, all 4 nozzles are designed identically and a 5<sup>th</sup> dummy nozzle is used for adaptation of the test conditions. A geometrically independent exhaust nozzle makes it possible to simulate one further similarity parameter in addition to the jet *pressure ratio* and the *turning angle similarity*. And, the geometry of the analysed nozzles remains unchanged from *start* to *cruise phase* as long as  $\kappa$ , R and  $T_{0,CC}$  remain constant regardless of a change in  $p_{0,CC}$ . The different combustion chamber pressure is realised by changing the cross-section of the independent nozzle.

For safety reasons, an over-pressure release is required in the model. This is to be placed in the base area and requires a central flow channel from the combustion chamber to the base. This enables a concept with a 5<sup>th</sup> central nozzle. The hot gas exit of this nozzle is expected to be so far downstream of the thrust nozzles that a backward influence on the flow conditions is not expected.

An analysis is performed for both types of propellant (2%/4% Aluminium) and finally a combination of both concepts is realised. The diameter of the thrust nozzle throat is set to  $D_{nt}=4.13\ mm$  and at the exit to  $D_{ne}=7.45\ mm$ . This gives a jet Mach number of  $Ma_j=2.50$ . Depending on the flight phase to be simulated and the propellant used, up to two thrust nozzles have to be exchanged by auxiliary nozzles with different throat area and/or a central nozzle has to be installed. An overview on the different combinations and on the dimensions of thrust, auxiliary and central nozzle is given in Table 1. With this concept, theoretically, the deviation in jet *pressure ratio* is < 2%, in *turning angle similarity* < 3% and in *momentum similarity* < 1%, based on the empirically derived relations.

		Thrust nozzle			Aux. Nozzle			Central Nozzle		
Phase	Propellant	#	D <sub>nt</sub>	D <sub>ne</sub>	#	D <sub>nt</sub>	D <sub>ne</sub>	#	D <sub>nt</sub>	D <sub>ne</sub>
Start	2%, 1G.	3	4.13	7.45	1	4.44	7.45	-	-	-
Interm.	2%, 1G.	4	4.13	7.45	-	-	-	1	5.39	9.66
Cruise	2%, 1G.	4	4.13	7.45	-	-	-	1	9.45	10.72
Start	4% 2G.	3	4.13	7.45	1	3.14	7.45	-	-	-
Interm.	4% 2G.	4	4.13	7.45	-	-	-	1	3.93	7.11
Cruise	4% 1G.	2	4.13	7.45	2	3.42	7.45	_	_	_

Table 1. Parameter of the hot gas nozzles (all dimensions in mm)

# Nozzle implementation in the wind tunnel model

Inclination angle of the thrust nozzles is  $\delta=22.5^\circ$ . For the *cold gas model*, the cross-sections in the nozzle throat and at the nozzle exit are realised by a simple cone nozzle with a 6° convergence and 10° divergence angle (Fig. 5, left). Air supply is from below. As the nozzles exit the model at an angle, the required exit cross-section is set perpendicular to the longitudinal axis of the nozzles at the upstream lip (see figure). Theoretically, the design jet Mach number  $Ma_j$  is reached in this cross section. All four thrust nozzles are realised in the nozzle segment of the model made from Inconel by selective laser melting and consecutive electric wire cutting. Individual or multiple nozzles can be blocked by fitting an insert in the air supply below the nozzle segment.

Implementation into the *hot gas model* made from Inconel is more complicated as, due to wear and tear, exchangeable inserts of graphite are required that contain the nozzle throat sections. As contour, again, a simple cone nozzle is chosen. The thrust nozzles have a 6.8° convergence and 10° divergence angle. The final part of each nozzle is hosted in the Inconel part. The design is shown in Fig. 5, right. The central nozzle can be closed with a metallic insert. Additionally, to protect from over-pressure, rupture discs are installed on four channels in this model part.

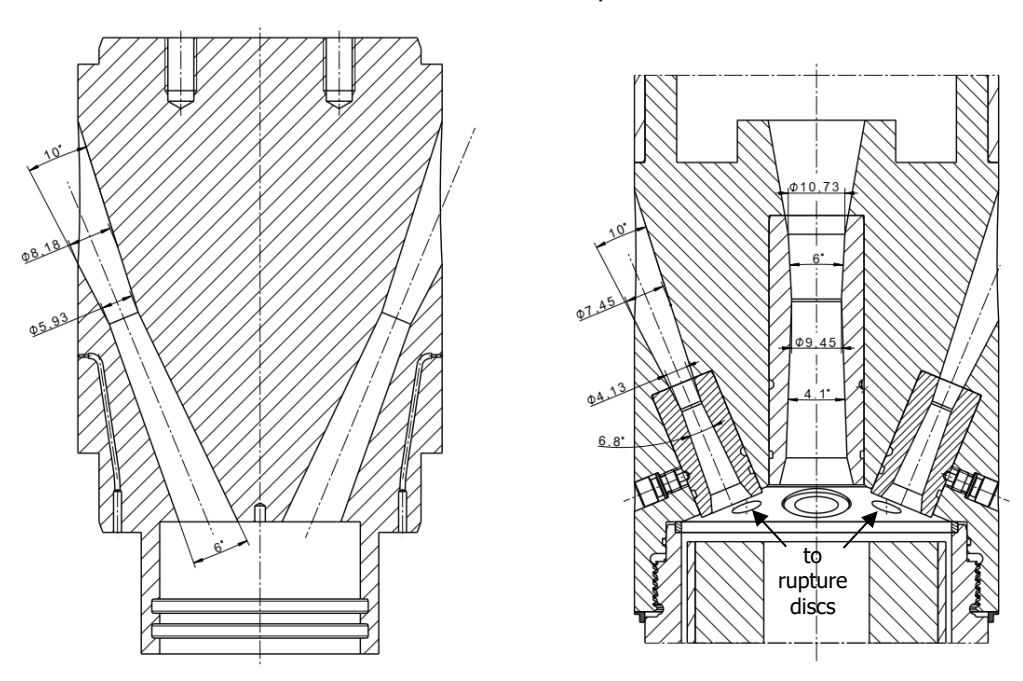


Fig. 5. Nozzle design of cold gas (left) and hot gas model (right)

## Implementation of the models into the wind tunnel nozzle

The wind tunnel models in the subsonic VMK nozzle are sketched in Fig. 6. The central model support in the nozzle allows for the supply of cold air and for the guidance of pressure measurement lines to the about 100 pressure ports of the *cold gas model* (left). In case of the *hot gas model*, ignition of the solid propellant is triggered from upstream via a glow plug in the combustion chamber's base that also contains a KULITE pressure sensor to measure the combustion pressure and a thermocouple for structural temperature surveillance. Electrical connections are guided to the outside via the central model support. Additionally, an air supply with external pressure measurement is connected to purge the combustion chamber from residues after each test.

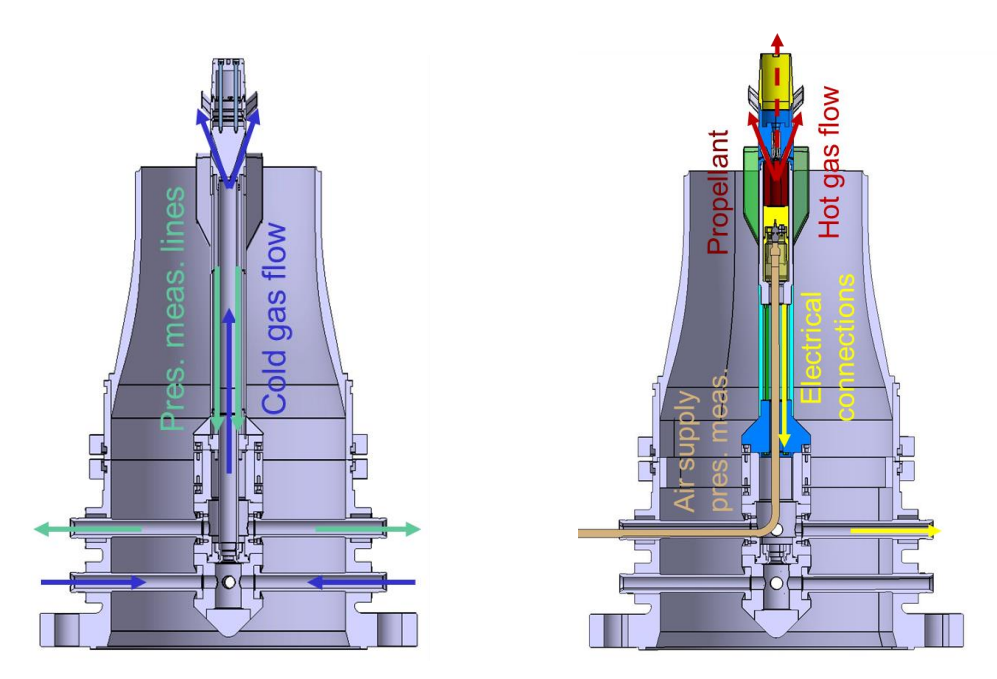


Fig. 6. Cold gas (left) and hot gas model (right) in subsonic VMK nozzle

# 2.3. MEASUREMENT TECHNIQUES

## Schlieren technique

In supersonic flows, shock waves and expansion fans can be made visible using the Schlieren technique. This involves passing parallel light through the test section, refocusing it before it reaches the camera, and using a knife edge to block light deflected by density gradients (caused by refractive index changes). Areas where light is blocked appear dark in the image. In the Schlieren images shown in this report, these dark regions correspond to shock waves or weaker disturbances known as Mach lines. Depending on the camera system either high-resolution images at low acquisition rate or low-resolution images at high acquisition rate are captured.

### Pressure Sensitive Paint

Pressure Sensitive Paint (PSP) is a measuring method for visualizing the pressure distribution on surfaces without sensors or probes interfering with the flow field. For this purpose, a thin layer of paint is applied to the surface in which fluorescent molecules are bound in an oxygen-permeable matrix. The molecules are excited with light of a suitable wavelength (e.g. ultraviolet light) and the fluorescent light is recorded with the aid of cameras. These are equipped with bandpass filters matched to the emitted wavelength. The fluorescent light is partially quenched, i.e. extinguished, in the presence of oxygen. If the local pressure increases, this leads to an increased oxygen concentration and thus to a decrease in the fluorescent light component detected at this point. This results in different degrees of brightness on the surface, whereby the measured intensity is inversely proportional to the locally prevailing pressure.

In addition to the pressure dependency of the light intensity, there is also a temperature dependency depending on the PSP paint used. If changes in the surface temperature occur when using the measurement method, this should therefore also be recorded and considered in the evaluation. To enable this, sample plates are prepared during the painting procedure of the model that later serve for a calibration of the paint in the full pressure and temperature range in a dedicated test stand. Thereby, the sensitivity of the paint with respect to temperature and pressure can be expressed in corresponding relations.

# Infrared technique

Temperature measurement is performed with commercially available infrared cameras that are equipped with IR-sensitive sensors. Surface temperatures can be determined relatively accurate if the emissivity of the material is known, but the temperature of a fluid (e.g. the exhausted hot gas jet) are usually not determined correctly. Nonetheless, the IR-visualisation of a fluid can contain relative information that serves in identifying structures like shock waves in supersonic flows. The IR-technique is applied to measure the surface temperature during PSP testing and for a visualisation of the IR signature of hot gas thrust jets. Temperature scales are omitted when presenting these IR images as only relative information can be gathered.

#### Pressure measurement

A DTC Initium system from PSI with four ESP-32HD scanners is used to record the pressures at the approx. 100 pressure ports on the model's surface. The scanners have 32 differential pressure sensors in the range of (2x) 100, 200 and 700 kPa. According to the data sheet, the accuracy of the pressure measurement is  $\pm 0.05\%$  of the sensor's range. The sensors are connected to the measuring points of the model via pressure tubes. The reference side is connected to one common pressure reference that is kept at atmospheric pressure. Thus, differential pressures between the pressure port and the reference are measured by the pressure scanners and absolute values calculated in the post-processing. These pressure data are used to check for an offset of the pressure values derived by PSP-measurement.

# Particle Image Velocimetry

Particle Image Velocimetry (PIV) is a contactless method for measuring velocities in flow fields. For its application, particles are introduced into the flow, so-called tracer or seeding particles. These must be so small that they follow the local flow direction and fully adapt to the velocity of the surrounding fluid.

With help of a pulsed laser and suitable optics, a light sheet is created in the flow field. The laser light is scattered by the particles located in this area so that they become visible. By recording images at fixed intervals, the direction of movement and the speed of the particles can be determined based on the distance travelled using PIV evaluation methods.

In the current case, two laser pulses and recording of double images are used. The cross-correlation method is applied in the evaluation, in which defined areas of both images are correlated with each other and the velocity information is derived from this. In addition, two identical camera systems are used, which record the same section in the light sheet from different directions. In this way, it is possible to determine all three components of the velocity vectors.

#### 3. EXPERIMENTS

In a first step, the pressure distribution on the model surface and the velocity field in and around the exhausted jet(s) are investigated with the cold gas model. The PSP- and PIV-technique are applied in consecutive test campaigns. Then, the velocity field of an exhausted hot gas jet is researched using PIV and IR technique. Schlieren visualisation is applied in every test.

Using the PSP-technique, two types of test are performed. First, with only a single thrust nozzle active and the other three nozzles blocked, the circumferential impact of the jet on the pressure distribution is investigated by successively rotating the model on the support by  $\Phi=90^\circ$ . Second, all nozzles activated allows for a simulation of the flight case. As result, the pressure coefficient  $c_p$  is presented that is calculated as

$$c_p = \frac{p - p_{\infty}}{q_{\infty}} \tag{4}$$

with p the measured local pressure value and  $p_{\infty}, q_{\infty}$  the static and dynamic pressure of the free stream.

In contrast, the PIV measurements focus on the velocity field in and around one jet. As seeding of wind tunnel and jet flow is performed, just one nozzle is activated and seeding of the wind tunnel restricted to the section around the jet. This increases testing time until concentration of seeding in the open test section of VMK passes a critical level and the test has to be aborted. The model is successively rotated on the model support by  $\Phi=5^\circ$ . As result, the velocity vector field is shown colour coded by the absolute velocity |V|.

In case of hot gas PIV tests, the desired test conditions could only be achieved with all 4 or even 5 thrust nozzles active (see Table 1). As two different types of solid propellant are used, the number of test conditions is reduced and investigations are only performed on the symmetry plane of the exhausted jet.

#### 3.1. TEST MATRIX

The experiments cover the full flight Mach range of LK6E2 from Ma=0 to Ma=0.9. An overview of the tests is given in Table 2. As indicated, PSP- and PIV-tests with the cold gas model cover the complete matrix whereas hot gas PIV (hgPIV) is performed mainly at Ma=0.7 and Ma=0.85.

	Start		Interm.			Cruise			off		
Ma	PSP	PIV	hgPIV	PSP	PIV	hgPIV	PSP	PIV	hgPIV	PSP	PIV
0	Х	-	-	Х	-	ı	Х	1	1	Х	-
0.3	Х	0°	-	Х	0,15°	ı	х	0°	1	Х	-
0.5	Х	0°	-	Х	0°	ı	х	0°	2%	Х	-
0.7	Х	0-20°	2/4%	Х	0-10°	2/4%	х	0-10°	2/4%	Х	-
0.85	Х	0-20°	2/4%	Х	0-10°	2/4%	х	0-10°	2/4%	Х	0,10°
0.9	Х	0-20°	-	Х	0-10°	ı	х	0-10°	1	Х	-

Table 2. Test matrix

Nomenclature
hg hot gas
0° symmetry plane
10°,15° model angle φ
0-10°/0-20° model turned
in 5° steps

# 4. EXPERIMENTAL RESULTS

In the frame of this paper, only a selection of results can be presented. The analysis is therefore restricted to a test Mach number of Ma=0.85. Data from the different tests are presented for the start and cruise phase condition. In hot gas testing, only results of the 2% Al propellant are shown.

#### 4.1. COLD GAS TESTS

# Pressure Sensitive Paint

Visualisation of the exhausted cold gas jet by means of Schlieren optics is shown in Fig. 7 together with the surface pressure distribution in terms of the pressure coefficient  $c_p$ , derived from PSP measurements. Schlieren images were recorded with  $12500\,s^{-1}$ , 1090 images per test condition and averaged images calculated that represent a duration of  $0.0872\,s$ . These images allow for an analysis of the occurring density gradients, but keeping in mind that the Schlieren technique gives an integrated information along the path of light, i.e. across the whole flow field.

On the left, the start condition with a design jet Mach number of  $Ma_j=2.14$  is shown. The set pressure ratio yields a so called "under expanded jet" that further expands after exit of the nozzle. Typical elements of this "inclined supersonic jet in cross-flow" are the bow shock that surrounds the jet on the upstream side and a following barrel shock (see Fig. 7, left). The jet starts deteriorating further away from the model when mixing with the surrounding flow field with Ma=0.85.

Next to the Schlieren image, the surface pressure distribution for this test condition is shown. The pressure coefficient  $c_n$  is calculated from the PSP measurement where 25 images were recorded at a

frequency of  $5~s^{-1}$ , averaged and processed together with the recorded surface temperatures by means of an IR camera. Thus, the pressure field is averaged over a testing time of 5~s. The colour coding indicates if the local pressure is above (bright, positive  $c_p$ ) or below (dark, negative  $c_p$ ) the static pressure of the free stream  $p_{\infty}$ . Deliberately, the grey scale was chosen as it visualises best the complete pressure range.

The exhausted jet yields a region of increased pressure upstream and of decreased pressure in a heart-like shape right downstream of the nozzle exit. Additionally, a thin line indicating a pressure gradient is visible, that originates downstream of the nozzle and curves towards the fin. There are other low pressure regions visible further downstream on the main body and, additionally, on the fin in parallel to leading and trailing edge indicating contour changes. The two spots on the fin represent markers that were used for projection of IR- and intensity images on the 3-D surface of the model.

On the right of Fig. 7, Schlieren image and pressure distribution for the cruise condition are shown. This time, the reduced pressure ratio yields an over expanded jet with a static pressure below the pressure of the free stream. This impacts on the shock wave structure and the penetration path of the jet into the cross-flow. As visible, a structure of successive shock waves is formed, like in a shock train, and the jet stays in the vicinity of the model surface.

In the pressure distribution, the regions of increased and decreased pressure up- and downstream of the nozzle are far less extent than at start condition, but it seems as if downstream of the nozzle, the oscillating jet pressure is projected onto the model surface giving an alternating pressure field. On the fins, the gradients appear slightly weaker than at start condition. This indicates that the jet at start condition slightly impacts on the pressure distribution on the fins.

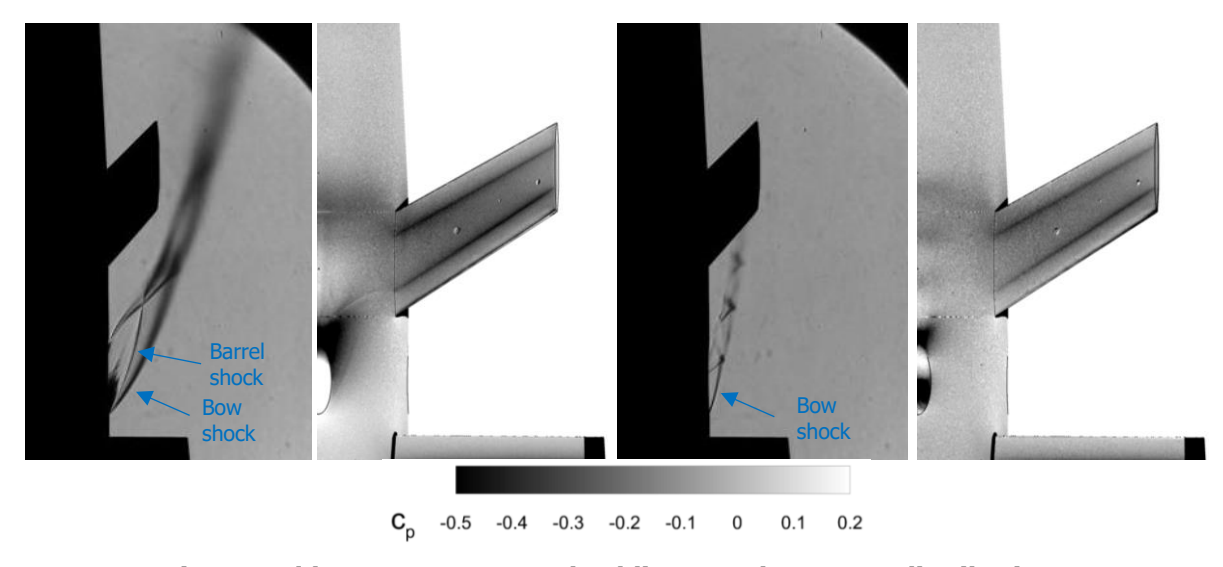


Fig. 7. Cold gas test: Averaged Schlieren and pressure distribution  $c_p$  left: Start cond.,  $p_{0,cc}=4.0~MPa$ , right: Cruise cond.,  $p_{0,cc}=0.9~MPa$ 

To further analyse the surface pressure field, the pressure coefficient is extracted along straight lines, once along the symmetry plane ( $\Phi=000^{\circ}$ ) and once from a plane rotated by  $-45^{\circ}$  around the longitudinal axis to  $\Phi=315^{\circ}$ . In both planes, pressure ports are existent and a comparison for assessment of a PSP offset is possible. The extracted PSP-data and the pressure port values for start (left) and cruise condition (right) are plotted together in Fig. 8. On the abscissa axis, the x-coordinate in meters is plotted, that originates in the model's nose and points upstream. The grey area indicates the missing part of the exhaust nozzle on the symmetry plane between X=-0.51421~m and X=-0.54129~m. Data for the symmetry plane are plotted in red, for the  $\Phi=315^{\circ}$  slice in blue.

Far upstream of the exhausted jet, pressure distribution on the model surface is found homogeneous with  $c_p \approx 0$  at both conditions. Then, both planes show a different pressure development along the X-coordinate, but the PSI and PSP data are always in quite good coincidence. It becomes obvious that

the PSP-technique reveals much more details here than could be derived from the PSI-measurement at discrete pressure ports. E.g. the pressure oscillation in the mid plane downstream of the exhausted jet is found with relatively high amplitude at start condition. At cruise condition, the amplitude is much smaller, but more maxima and minima are found in the "footprint of the shock train". This was already observed in the field plot of Fig. 7.

The complete investigation with the LK6E2 cold gas model by means of Pressure Sensitive Paint is published in [4].

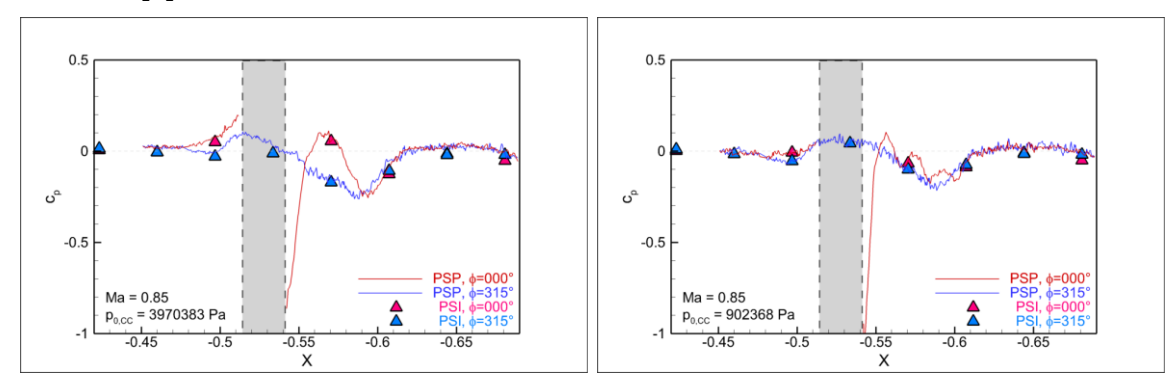


Fig. 8. Pressure distribution  $c_p$  in longitudinal direction from PSI and PSP measurement left: Start cond.,  $p_{0.CC} = 4.0 \, MPa$ , right: Cruise cond.,  $p_{0.CC} = 0.9 \, MPa$ 

### Particle Image Velocimetry

The results from the PIV-measurements for start and cruise condition are plotted in Fig. 9. This time, an instantaneous Schlieren image is shown although the derived velocity fields represent an averaged flow field. (For comparison with averaged Schlieren, refer to Fig. 7.) Double images in a stereoscopic setup with approx.  $70^{\circ}$  between the camera axis (observing the light sheet from different sides) are recorded with  $15~s^{-1}$  and processed individually. Then, the flow field is averaged across 100 recordings, i.e. across 6.67~s, and plotted on top of the Schlieren image. Although, the model was painted in black, reflexion of the light sheet on the model disables any velocity measurement near the surface.

At start condition (Fig. 9, left), the combustion chamber pressure of  $p_{0,CC}=4.0~MPa$  exceeds the operating limit of the seeding generator. Therefore, the jet stream could not be enriched with particles, but estimation of velocity data in the jet becomes possible when mixing of the jet with the free stream sets in. So only the initial part of the jet is missing. In the free stream, the derived velocity is about  $V_{\infty} \approx 245~m/s$  and thereby slightly below the theoretical value of  $V_{\infty,th.} \approx 266.5~m/s$ , calculated from the stagnation conditions with gas dynamic relations. The jet structure with its constriction is well resolved in the PIV measurement. In the jet, velocities up to  $V_j \approx 550~m/s$  are found upstream and downstream of the constriction, proving a further acceleration of the jet above the theoretical velocity at nozzle exit of  $V_{i,th.} \approx 518.6~m/s$ .

The results for the cruise condition are shown in Fig. 9, right. As the exhausted jet is enriched with particles, velocity data can be derived right from the nozzle exit. The free stream velocity is again found around  $V_{\infty} \approx 245 \, m/s$ , except further away from the model where the lower seeding density limits a proper image processing. In the jet, an alteration of the velocity is found that corresponds well with the shock structure visible in the Schlieren image (see also Fig. 7, right). A successive deceleration and re-acceleration take place whereby the velocity observed at maximum with  $V_j \approx 475 \, m/s$  is below the theoretical value at nozzle exit of  $V_{j,th} \approx 518.6 \, m/s$ . This corresponds with the expectations for an over expanded jet that is decelerated in the cross-flow.

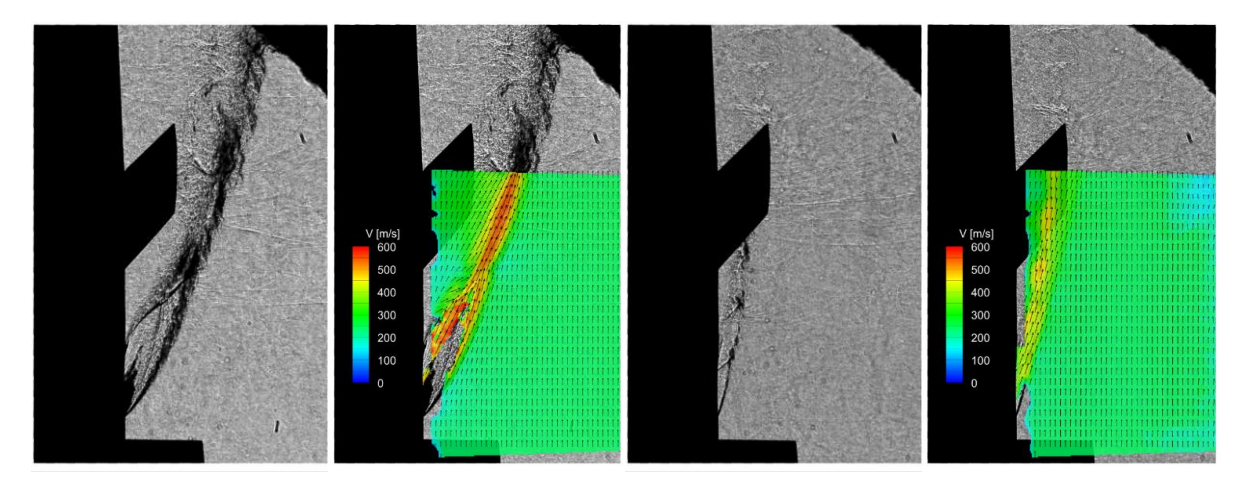


Fig. 9. Cold gas test: Instantaneous Schlieren and averaged velocity field Ma = 0.85, left: Start cond.,  $p_{0.CC} = 4.0 \, MPa$ , right: Cruise cond.,  $p_{0.CC} = 0.9 \, MPa$ 

The presented results concentrated on a flight Mach number of Ma=0.85, but similar analysis have been performed for all recorded test data. In conclusion of the cold gas testing it can be stated that the three measurement methods Schlieren, PSP and PIV provide complementary results across all tested conditions. This enables a comprehensive analysis of the flow field around the thrust jet for the complete flight envelope of LK6E2.

#### 4.1. HOT GAS TESTS

Combustion of the solid propellants does not yield a constant combustion chamber pressure, but leads to a certain pressure evolution over time. One grain with 2% Al-content gives a combustion phase of less than 1 s whereby one grain with 4% Al-content gives a phase of up to 5 s. In the post processing, timing signals have to be accurately adjusted to enable comparison of different signals. This is still in progress so that only preliminary results are presented hereafter.

# Infrared technique

Schlieren and IR images give an insight into the flow structure of the exhausted hot gas jet. In Fig. 10, both are presented for tests at Ma=0.85 with start condition (left) and cruise condition (right). The pressure in the combustion chamber reaches at maximum  $p_{0,cc}=8.23~MPa$  for start condition with the central nozzle blocked and  $p_{0,cc}=1.72~MPa$  for cruise condition with an active fifth nozzle. In the right IR-image the hot model base, caused by the hot gas exhaust via the central nozzle, is visible to some extent at the image's top.

Schlieren images were recorded with  $12500\ s^{-1}$ , but, as pressure alters during the test, an average across only 100 images is built representing a test time of  $0.008\ s$ . As combustion of the solid propellant produces  $Al_2O_3$ -particles, the density gradients in the Schlieren images experience some "shading and blurring" as light is partially blocked and scattered by the particles. At start condition, the bow shock is clearly visible in the image, but also the following barrel shock. Comparison to the cold gas case (Fig. 7, left) reveals a slightly different path of the bow shock and a slightly higher penetration depth of the jet into the free stream. But in the whole, a resembling shock structure is found. Same accounts for the cruise phase (right) with the over expanded jet, forming a system of successive shock waves in both, the cold and the hot gas case.

To some extent, the shock structure is also visible in the IR-images where the highest temperatures are recorded at the exit and at approx. the position of the shock intersection. At start condition, the IR-map shows that the jet splits on its path downstream when mixing with the free stream sets in, shortening the IR-signature of the jet. At cruise condition, the plume of the jet is narrower, but its extension longer. Temperature level is comparable for both conditions.

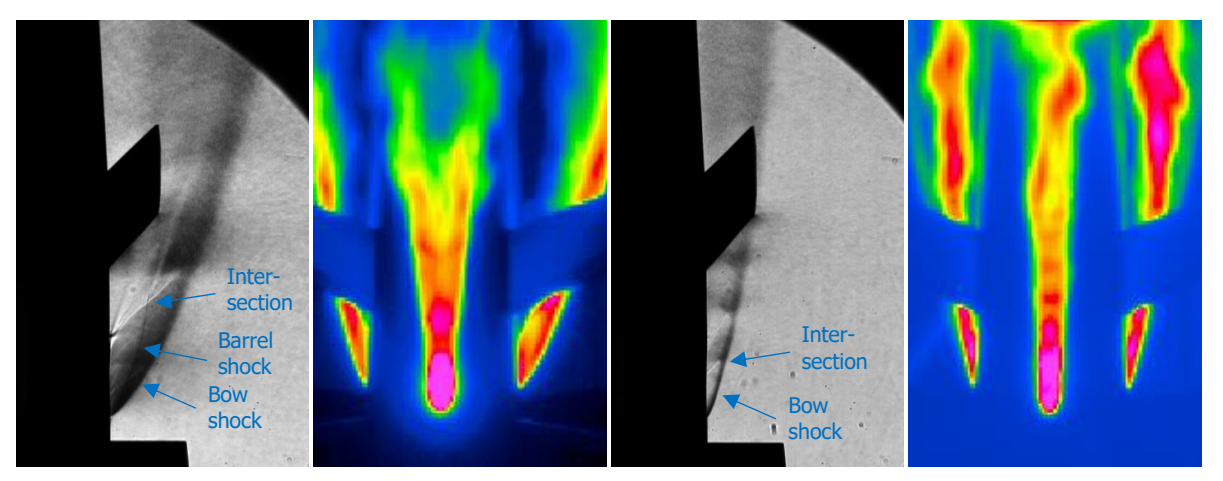


Fig. 10. Hot gas test, 2%Al: Averaged Schlieren and IR-image Ma=0.85, left: Start cond.,  $p_{0,CC}=8.23\,MPa$ , right: Cruise cond.,  $p_{0,CC}=1.72\,MPa$ 

# Hot gas Particle Image velocimetry (hgPIV)

The recording of double images with a stereoscopic setup is performed again with a recording frequency of  $15\ s^{-1}$ . Thus, for the propellant with 2% Al-content, only 10-12 image pairs exist, all recording the jet at a slightly different combustion chamber pressure. Therefore, averaging is no option in the hot gas PIV evaluation process. Additionally, the particle density in the jet and the surrounding free stream is extremely different which requires a high effort in pre-processing of the images, before the PIV-algorithms can be applied. As this phase of image evaluation is still ongoing, hereafter preliminary results from a single camera evaluation (not stereoscopic) are presented, correlated with the corresponding instantaneous Schlieren images.

On the left side of Fig. 11, the results for the start phase and on the right side for the cruise phase are presented. Obviously, in both cases, the level of turbulence is higher than with cold gas which makes other jet shock structures than the bow shock barely visible in the instantaneous images. The determined velocity fields are drawn on top of the Schlieren images to demonstrate that the silhouette of the jet as well as the penetration depth are quite good in correspondence. As the high turbulence level impacts on the velocity measurement and no averaging is performed, there is a high alteration in the data field. The velocity determined in the free stream is in the range of  $250 \le V_{\infty} \le 280 \, m/s$  for the start condition and of  $230 \le V_{\infty} \le 270 \, m/s$  for the cruise condition, which is both around the calculated velocity of  $V_{\infty,th.} \approx 266.5 \, m/s$  at Ma = 0.85.

The under expanded jet at start condition experiences a further expansion after the nozzle exit, reaching velocities of up to  $V_j \approx 2200~m/s$ . In theory, the expansion of the hot gas of the 2% Al solid propellant to  $Ma_j = 2.5$  gives a velocity at the nozzle exit of  $V_{j,th.} = 2043.6~m/s$ , but the uncertainty of this value is quite high as the temperature of the exhaust gas can only be estimated. In case of the cruise condition, the over expanded jet is immediately decelerated via a shock wave system after nozzle exit and velocities only up to  $V_j \approx 1850~m/s$  are measured. The shock train like structure is slightly visible in the determined velocity field.

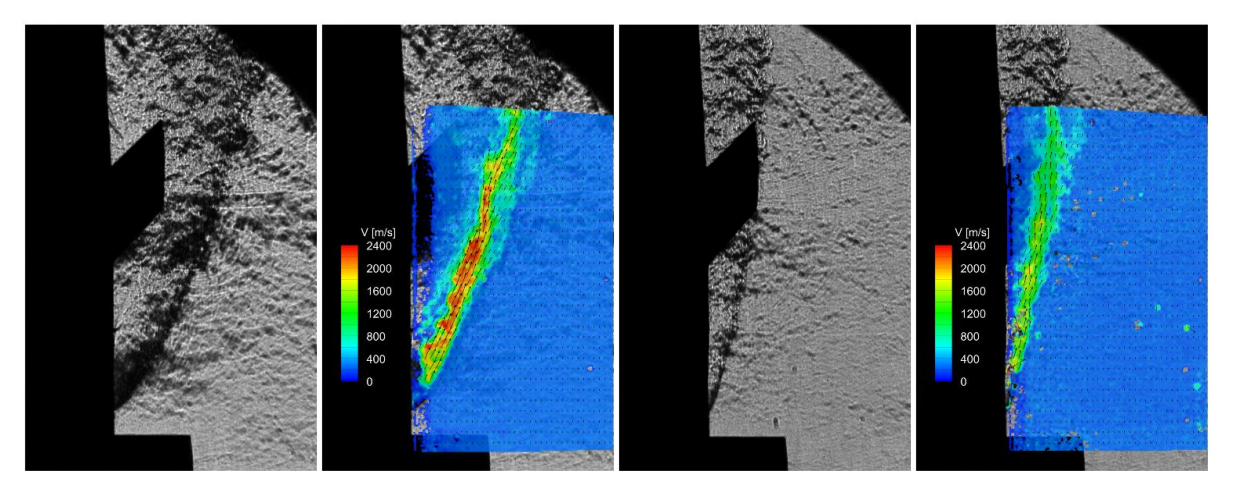


Fig. 11. Hot gas test, 2%Al: Instantaneous Schlieren and velocity field Ma = 0.85, left: Start cond.,  $p_{0.CC} = 8.23 \, MPa$ , right: Cruise cond.,  $p_{0.CC} = 1.72 \, MPa$ 

Evaluation of the hgPIV tests is quite challenging, especially as a high effort in image pre-processing is required to allow for an application of PIV algorithms. Additionally, an accurate timely correlation between the recorded combustion chamber pressure  $p_{0,cc}$  and the PIV images is necessary. The analysis is still ongoing and further results can be expected soon.

#### 5. CONCLUSION

The LK6E2 was designed by DLR as a subsonic missile configuration that is boosted by solid propellant via four thrust nozzles circumferentially arranged at the missile's tail. The followed approach in the current study was to first perform experiments with an exhausted cold gas jet and then extend the investigation on a hot gas jet, well knowing that the composition of the propellant would be different to the real one. Application of similarity rules to the thrust nozzle design for cold and hot gas model should allow for results of the different experiments being transferable to the real configuration.

All tests were performed in the vertical test section VMK. Different measurement techniques were applied to investigate the flow structure, velocity field and surface pressure distribution in vicinity of the thrust jet. As outcome of the study, the chosen approach has proven successful in general, but with minor deficiencies on certain details. The flow structure of cold and hot gas experiments is comparable up to a certain extent and the velocity fields correlate qualitatively. Therefore, it is assumed that the pressure distribution determined from cold gas experiments can also be transferred qualitatively to the hot gas case or the real configuration. Thereby, the chosen approach seems to yield the results aimed by the current study.

The analysis of experimental data is still ongoing and also a comparison to numerical simulation data is aimed. Finally, a comprehensive evaluation of the thrust jet characteristic at different flight phases and of the interaction between jet and control surfaces is planned. Most likely for this interaction seems the start phase with its high thrust level and primarily an interaction with the control surfaces that are closer to the jet due to the circumferential arrangement of the fins. PSP results were not presented for these surfaces herein as the aim of this publication was more to give an overview about the vast experimental program by presenting correlated results than to go deep into a certain detail. This could be the topic of another future publication.

#### 6. REFERENCES

- [1] P. Gruhn and C. Schnepf, "Referenzdaten zur Bewertung mittels semi-empirischer Tools ermittelter Flugkörperaerodynamik-Beiwerte," in "Beitrag DLR zur Studie "Hyperschall-FK-Aerodynamik" (E/K2/AH/KA069/JF008)," Institut für Aerodynamik und Strömungstechnik, 12. Oktober 2020.
- [2] D. Saile, "Experimental Analysis on Near-Wake Flows of Space Transportation Systems," in "Forschungsbericht," Rheinisch-Westfälische Technische Hochschule Aachen (RWTH), Dissertation 2019, vol. 2019. [Online]. Available: <a href="https://elib.dlr.de/130993/">https://elib.dlr.de/130993/</a>
- [3] M. Pindzola, "Jet Simulation in Ground Test Facilities," in "AGARDograph 79," North Atlantic Treaty Organization, Advisory Group for Aeronautical Research and Development, Paris, 1963.
- [4] T. Gawehn, "Untersuchungen zur Schubstrahlinteraktion an einem Unterschallflugkörper mit Hilfe von Pressure-Sensitive-Paint," Institut for Aerodynamics and Flow Technology, Cologne, Internal Report DLR-IB-AS-KP-2022-143, 01. Dezember 2022. [Online]. Available: <a href="https://elib.dlr.de/192084/">https://elib.dlr.de/192084/</a>